

Design of a high-frequency transformer based on amorphous cut cores for insulation breakdown testing

Lagerweij, Gijs; Niasar, Mohamad Ghaffarian

DOI

[10.1049/hve2.12460](https://doi.org/10.1049/hve2.12460)

Publication date

2024

Document Version

Final published version

Published in

High Voltage

Citation (APA)

Lagerweij, G., & Niasar, M. G. (2024). Design of a high-frequency transformer based on amorphous cut cores for insulation breakdown testing. *High Voltage*, 9(5), 1183-1194. <https://doi.org/10.1049/hve2.12460>

Important note

To cite this publication, please use the final published version (if applicable). Please check the document version above.

Copyright

Other than for strictly personal use, it is not permitted to download, forward or distribute the text or part of it, without the consent of the author(s) and/or copyright holder(s), unless the work is under an open content license such as Creative Commons.

Takedown policy

Please contact us and provide details if you believe this document breaches copyrights. We will remove access to the work immediately and investigate your claim.

ORIGINAL RESEARCH

Design of a high-frequency transformer based on amorphous cut cores for insulation breakdown testing

Gijs Lagerweij¹  | Mohamad Ghaffarian Niasar² 

¹Prodrive Technologies, Son, The Netherlands

²High Voltage Technologies, Electrical Sustainable Energy, Delft University of Technology, Delft, The Netherlands

Correspondence

Mohamad Ghaffarian Niasar, Delft University of Technology, Mekelweg 4, Delft 2628 CD, The Netherlands.

Email: m.ghaffarianniasar@tudelft.nl

Associate Editor: Fan Yang

Funding information

TKI Urban Energy, Grant/Award Number: 1821403

Abstract

Innovative test methods are required to keep up with the increased demand for insulation materials which can withstand the high-frequency square-wave voltages generated by power-electronic equipment. Test systems using high-voltage, high-frequency transformers have proven versatile and easy to realise. The authors investigate the application of amorphous cut cores in such transformers. Analytical and numerical models for the transformer and its frequency response are developed, aiding the design process. An amorphous core-based transformer is designed for 8 kV_{pk} output at 100 kHz and compared to two previous designs based on ferrite cores. The frequency and pulse response, as well as the high-voltage and thermal performance, are evaluated. The comparison shows that while the low parasitics of the amorphous-based transformer allow for superior frequency response, they are unsuitable for long-duration tests with high pulse repetition frequencies (25–100 kHz) due to increased core losses. The partial discharge inception and flashover voltage are comparable to the ferrite-based transformers.

1 | INTRODUCTION

Medium and high-voltage insulations are increasingly exposed to voltage waveforms with high-frequency (HF) content generated by power electronics (PE), which results in the rapid degradation of the insulation [1, 2].

Solid-state transformers (SST) are a critical component enabling the energy transition. SSTs are controlled by power-electronic converters and the major size advantage originates from a high operating frequency. The electrical and thermal aspects of SST insulation design must account for the effect of non-sinusoidal HF voltage stresses [3]. The effect of high-frequency stress was historically already appreciated in variable frequency drives because long connecting cables caused severe transient overvoltages. With the advent of wide-bandgap semiconductors, shorter rise times and higher switching frequencies enable more compact and efficient electric vehicles. However, this comes at the cost of increased HF voltage stress on the winding insulation [4, 5]. Finally, the introduction of high-voltage semiconductor devices in PE means that printed circuit boards will also be exposed to non-

sinusoidal HF high voltages. This introduces the risk of intense PD activity and degradation at relatively low voltages [6, 7].

Therefore, novel methods must be established to test and analyse the breakdown characteristics of insulation materials under representative PE stresses. Using such methods, the ageing mechanisms can be studied and translated to design guidelines to ensure a reliable operation of the equipment over its intended lifetime.

1.1 | Test methods

Several methods are being developed to test the breakdown of insulation materials with non-sinusoidal voltage waveforms. Those methods that allow for testing with square waves are of particular interest since these resemble the waveforms encountered in PE. The three critical parameters which must be achieved are (i) high output voltage, (ii) high frequency, and (iii) short rise times. The following three methods are used in literature to generate high-frequency (HF) high-voltage (HV) square waves.

This is an open access article under the terms of the [Creative Commons Attribution](https://creativecommons.org/licenses/by/4.0/) License, which permits use, distribution and reproduction in any medium, provided the original work is properly cited.

© 2024 The Authors. *High Voltage* published by John Wiley & Sons Ltd on behalf of The Institution of Engineering and Technology and China Electric Power Research Institute.

- Full- or half-bridge configurations with SiC MOSFETs can easily reach the desired frequency and rise time but are severely limited in output voltage. As a result, this method can only be used for testing low-voltage insulation. For example, Agarwal et al. use 3.3 kV SiC switches to test polyimide tape with 50 kHz and 60 kV/ μ s at a maximum voltage of 2 kV [3].
- Full- or half-bridge configuration with high-voltage switches allows for a higher output voltage but can typically not switch very fast. Mirza et al. have investigated the breakdown strength of polyimide tape up to 5 kV and 4 kHz using 33 kV high-voltage switches [4].
New developments in this direction are made using series/parallel-connected SiC MOSFET. This approach has shown promising results [8].
- High-frequency transformers can step up low-voltage pulses generated by an inverter to the desired high voltage, which allows for high-voltage, high-frequency output. Oil-impregnated paper has been tested by Mathew [9, 10] and Kaparapu [11] up to 10 kV at 50 kHz.

In this paper, the last method will be investigated. The general architecture of an insulation test system with an HF transformer is shown in Figure 1. The inverter generates low-voltage pulses (using a full-bridge topology), which are amplified by the transformer. Since insulation has predominantly capacitive behaviour, the load or device under test (DUT) is represented by a capacitance C_{DUT} . The rise time and overshoot can be tuned using R_d and C_d . Even a small amount of overshoot can affect the measured insulation lifetime. Therefore, this must be considered in the analysis.

1.2 | Contributions

The advantages and challenges of the HF transformer approach are examined to determine its scalability to higher voltages and frequencies. Most pulsed-power literature considers applications with a low-pulse repetition rate and a resistive (e.g. klystron) load, which are not representative of the intended usage.

From literature (e.g. [12]), it is found that the high leakage inductance of ferrite-based transformers imposes a limit on the achievable rise time when driving a capacitive load, which may be improved by selecting a core material with higher saturation induction B_{sat} . Therefore, the paper's primary goal is to present such an improved transformer design and compare it against ferrite-based transformers.

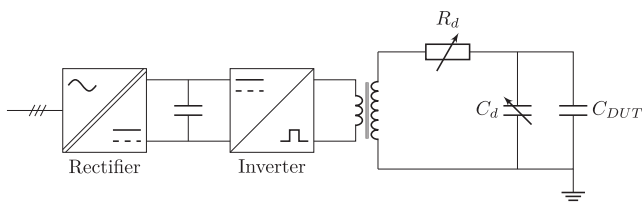


FIGURE 1 Insulation breakdown test setup utilising an LV inverter and HV HF transformer.

1.3 | Structure

First, an analytical analysis of HF transformer behaviour is presented, and the properties of the two magnetic core materials are compared. Second, a design procedure is outlined based on the presented analysis. An attempt is made to predict the characteristics of the designed HF transformer. Three transformer designs are presented, one of which is a new design based on an amorphous magnetic core. Finally, measurements are performed on the realised transformers to validate the models and comparison is made between the achievable performance with ferrite and amorphous cores.

2 | HF TRANSFORMER ANALYSIS

Although HF transformers allow for very high step-up ratios and hence high output voltages, the output voltage waveform can be severely distorted by its non-idealities. In this section, the frequency response of a transformer is modelled analytically, and a parameter extraction procedure is presented.

2.1 | Equivalent circuit

The equivalent circuit in Figure 2 is defined by the IEEE 390 standard to model the response of an HF transformer. Simplifications are recommended for three intervals: (i) rising flank, (ii) pulse top, and (iii) falling flank. These allow for approximate computation of parameters such as rise time, overshoot, and pulse droop.

The parasitic elements: leakage inductances L_{11} and L_{21} and parasitic capacitances C_{11} and C_{22} limit the bandwidth of the transformer. Resonances between these elements can result in overshoot and high-frequency ringing when driven by a rectangular pulse.

2.2 | Frequency response modelling

Besides looking for approximate solutions in the time domain, the transformer's frequency response can give valuable information. The higher the bandwidth, the steeper the pulses that can be recreated and the higher the repetition frequency. Peaks in the frequency response also indicate ringing and overshoot in the time domain.

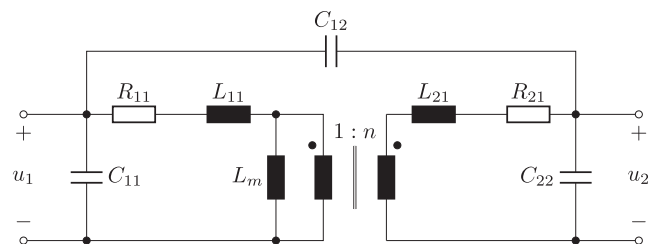


FIGURE 2 Equivalent circuit of a pulse transformer (IEEE 390 [13]).

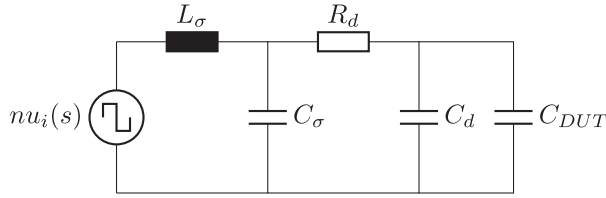


FIGURE 3 Simplified equivalent circuit of an HF transformer driving a capacitive load C_{DUT} through a damping circuit composed of R_d , C_d .

Using the simplified equivalent circuit in Figure 3, the output voltage u_{DUT} of a transformer driving a capacitive load is derived. The third-order Equation (1a) expresses the response in terms of the transformer parasitics P (stray inductance L_σ and capacitance C_σ), damping filter quality Q (comprising load capacitance and damping resistor R_d), and the coupling or ‘relational’ parameter R .

$$\frac{u_{DUT}(s)}{u_i(s)} = \frac{nPQ}{s^3 + s^2R + sP + PQ} \quad (1a)$$

$$P = \frac{1}{L_\sigma C_\sigma} \quad (1b)$$

$$Q = \frac{1}{R_d(C_{DUT} + C_d)} \quad (1c)$$

$$R = Q + \frac{1}{R_d C_\sigma} \quad (1d)$$

If the parasitic capacitance C_σ is very small compared to the load capacitance, it can be neglected to obtain a second-order damped RLC circuit with natural frequency ω_0 and damping ζ .

$$\omega_0 = \frac{1}{\sqrt{L_\sigma(C_{DUT} + C_d)}} \quad (2a)$$

$$\zeta = \frac{R_d}{2} \sqrt{\frac{C_{DUT} + C_d}{L_\sigma}} \quad (2b)$$

Although it appears that increasing L_σ or C_σ would result in a reduced bandwidth, a closer analysis of the PQR equation in Figure 4 shows that some amount of parasitic capacitance (up to 25–50% of $C_{DUT} + C_d$) reduces the rise time. This counter-intuitive fact is explained in the Appendix A.

2.3 | Parameter extraction

To evaluate the designs in this paper and compare them against the simulations, it is important to extract the parameters of the transformer through measurement. The method below is based on the procedure of Candolfi et al. [14]. An example of primary impedance measurement and simulation based on

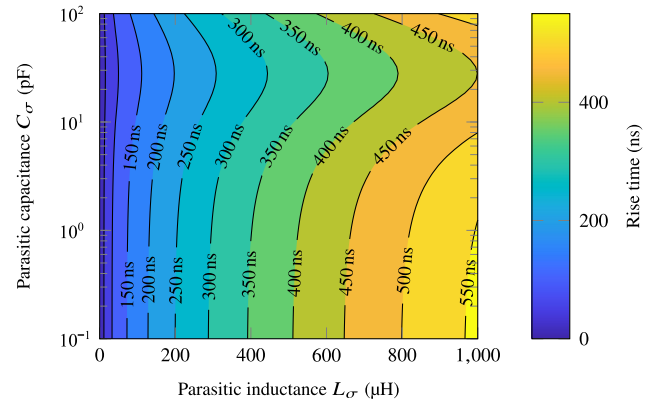


FIGURE 4 Map of rise time versus L_σ and C_σ with R_d tuned to give $\zeta \approx 1/\sqrt{2}$ for a load of 68 pF.

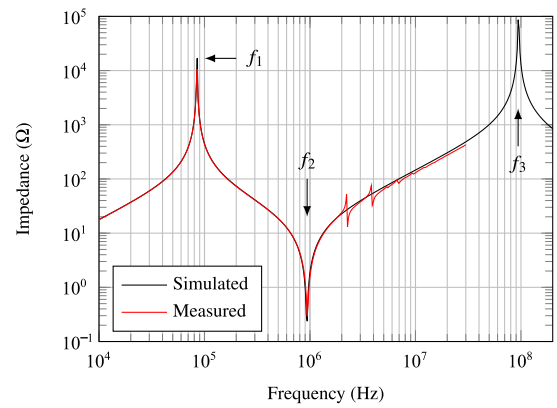


FIGURE 5 Primary impedance of PT2 measured with Bode 100 vector network analyser (VNA).

extracted parameters is shown in Figure 5. Transformer parameters are summarised in Section 5.1.

2.3.1 | Inductances

The magnetising inductance L_m can be measured using an LCR metre connected to the primary winding and the secondary open-circuited. For the leakage inductance L'_σ , the secondary should be short-circuited while measuring primary inductance.

2.3.2 | Capacitances

The winding capacitances C_{11} and C_{22} and inter-winding capacitance C_{12} must be measured using a vector network analyser (VNA) or from the oscillations in the pulse response. The resonance peaks in the primary impedance correlate to C'_{22} and C'_{12} (see Appendix).

$$f_1 = \frac{1}{2\pi\sqrt{L_m C'_{22}}} \quad (3)$$

$$f_3 = \frac{1}{2\pi\sqrt{L'_\sigma C_{12}}} \quad (4)$$

It is also possible to measure C_{12} between the windings using an LCR metre. In this case, the measured value must be divided by 3 [15] to account for the linear voltage distribution, which is not present during the capacitance measurement.

3 | MAGNETIC MATERIALS

The choice of magnetic core material will determine much of the properties and limitations of the HF transformer. A trade-off must be made between cost, volume, high-frequency performance, and efficiency. This paper considers two materials: ferrite and amorphous metal alloys.

3.1 | Ferrite

Ferrite is a ceramic material with small proportions of metallic elements, which determine its magnetic properties. Manganese–zinc (MnZn) is commonly used below 5 MHz because it offers superior permeability and saturation level compared to nickel–zinc (NiZn), which is used at higher frequencies.

Ferrite is the go-to material for magnetic components used in power electronic converters. It is cheap, has good high-frequency performance, and is available in various shapes and magnetic properties. MnZn cores have been used for HV HF transformers on several occasions [11, 16]. However, these typically have limited rise times in the order of 1–3 μ s.

3.2 | Amorphous metals

Amorphous metals have a saturation level much higher than ferrites but lower than silicon steel. However, they have good high-frequency performance because of their high resistivity and low coercivity. This combination of properties makes investigating their application in HF transformers interesting, mainly because it could reduce the number of turns and, consequently, the leakage inductance and rise time.

Recently, amorphous alloys have been used successfully in medium frequency (1–10 kHz) transformers for power levels of 2–40 kW [17, 18]. However, there is no literature describing their performance for frequencies between 10 and 100 kHz. Toroidal amorphous cores have been applied in an HV pulse transformer with a very low pulse repetition frequency for a resistive load [19].

3.3 | Material properties

In this paper, cores made of two materials are investigated. The ferrite cores are made of MnZn-based N87 ferrite with

dimensions UU93/152/30 and UU126/182/20. The amorphous cores are AMCC1000, made from an iron-based Met-Glas alloy. The magnetic and electrical properties of these two materials are summarised in Table 1. The saturation induction B_{sat} , coercivity H_c and relative permeability μ_r describe the shape of the BH curve. The resistivity ρ affects the high-frequency eddy current losses.

The core loss and BH curves are extracted from the datasheet and presented in Figure 6. The higher μ_r and B_{sat} of the amorphous metal are clearly visible in the BH curve. The core losses are also much higher than that of the ferrite material, as seen from the larger enclosed BH product. On a material level, the majority of the losses are due to hysteresis. After core processing, cuts and imperfections may lead to an increase in core loss due to eddy currents.

TABLE 1 Magnetic core material properties.

Property	Ferrite N87	MetGlas 2605SA1
B_{sat}	0.5 T	1.56 T
H_c	20 A/m	15 A/m
μ_r	2200	$\geq 10,000$
ρ	10 Ω m	1.3 $\mu\Omega$ m

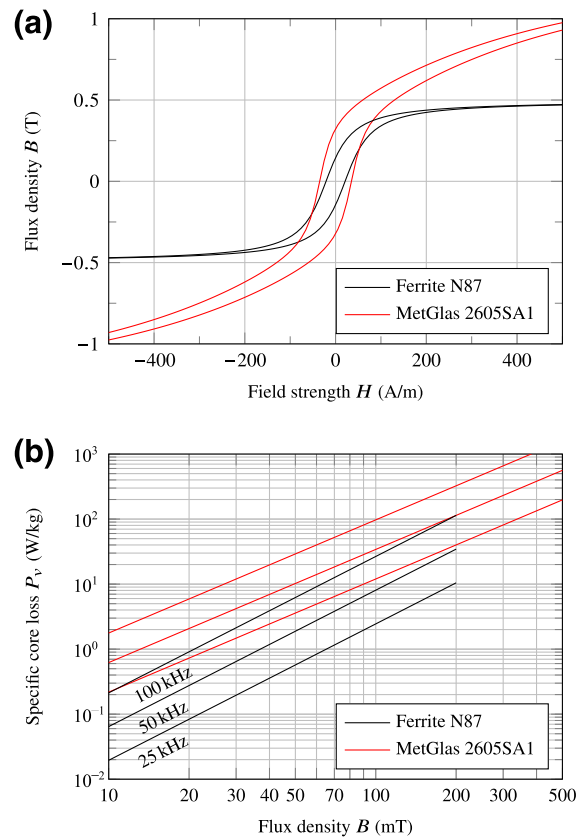


FIGURE 6 Properties of the N87 ferrite and MetGlas amorphous core materials. (a) BH characteristics at $f = 10$ kHz and (b) core loss curves for $f = 25$ kHz, 50 kHz, and 100 kHz.

3.4 | Challenges with amorphous cut cores

Despite their relatively high resistivity (e.g. compared to 96 nΩ m and 0.47 μΩ m for pure iron and 3% silicon steel, respectively), amorphous metals are manufactured as ribbons of several 10 s of μm thickness and laminated to reduce eddy current losses. After winding the ribbons, the core is vacuum-impregnated with epoxy and cut in half. Several challenges arise due to the cutting of the core:

1. At the location of the cut, short circuits will be created between laminations, resulting in large eddy currents, increased core losses, and a reduced effective μ_r . The short circuits are removed by etching the cut surfaces.
2. Because the surface of the cut will never be completely smooth, a small air gap will exist, further reducing the achievable effective μ_r .
3. The small air gap gives rise to a fringing flux which flows orthogonally to the core ribbon, inducing eddy currents and increasing core losses around the cut [20].

Because of this, typical values of effective μ_r are comparable to those of ferrite in the range of 1000–2000.

4 | DESIGN

In this section, the design procedure and considerations for HV HF transformers are discussed. In particular, the design focuses on reducing the transformer parasitics (L_σ and C_σ) to achieve the fastest possible rise time while maintaining a high output voltage. Other aspects, such as cost, weight, and size, are not considered.

4.1 | Design considerations

The design of an HF transformer for HV applications requires some additional attention. Most importantly, a trade-off must be made between the electrical performance and the HV aspects of the design (summarised in Table 2).

Flashover may occur between the transformer's magnetic core(s), low-voltage, and high-voltage winding. The designs

TABLE 2 Failure modes and mitigations.

Failure mode	Mitigation
I Core to LV discharges	Grounding the core; insulation between the core and LV winding
II HV to core discharges	Sufficient clearance; insulation between the core and HV winding
III HV to LV discharges	Sufficient clearance; insulation between HV and LV winding
IV Core to core discharges	Sufficient conductive contact between the core segments

below aim to minimise leakage inductance while ensuring no high-voltage-related failures can occur.

4.2 | Dimensioning

A turns ratio is derived based on the required input and output voltage. The minimum number of primary turns N_p can be calculated using the effective area A_e of the selected core, primary voltage U_p , and frequency f_s . The induction B_{\max} should be chosen well below B_{sat} to limit the core loss and prevent saturation.

$$N_p \geq \frac{U_p}{4B_{\max}A_e f_s} \quad (5)$$

Amorphous cores with high B_{sat} can have fewer turns than ferrite cores with the same area. However, note that the magnetising inductance L_m should remain large enough to prevent droop in the output waveform.

4.3 | Leakage inductance

The leakage inductance of the transformer can be estimated for a concentric winding configuration using Equation (6) [21].

$$L_\sigma = \mu_0 N_2^2 \left[\frac{l_{m1}d_1}{3b_1} + \frac{l_{m2}d_2}{3b_2} + \frac{l_{mg}d_g}{h_g} \right], \quad (6)$$

where μ_0 is the vacuum permittivity, d_1 , d_2 are the thicknesses of the windings, d_g is the dimension of the gap, b_1 , b_2 are the heights of the windings, $h_g = (b_1 + b_2)/2$ is the effective gap height, and l_{m1} , l_{m2} , and l_{mg} are the mean lengths of the windings and the gap. Fringing at the end of the windings can be included by reducing the winding height h by a factor K_R [21].

$$K_R = 1 - \frac{d_1 + d_2 + d_g}{\pi h} \left[1 - \exp\left(-\frac{\pi h}{d_1 + d_2 + d_g}\right) \right] \quad (7)$$

The leakage should be minimised to achieve the highest possible bandwidth (see Section 2.2), which can be done by

- Reducing the number of turns N , since the leakage inductance scales with N^2 .
- Reducing the turns ratio n . Referring L_{11} to the secondary side scales with n^2 .
- Reducing the volume between the windings, where most leakage field energy is stored. This can be achieved by making the windings the same height (increasing h_g) or bringing them closer together (decreasing d_g).
- Using a symmetrical arrangement of cores and windings.

The parasitic capacitance was found to have no significant detrimental effect on the rise time if it remains small compared

to the capacitance of the DUT. Depending on the other requirements, not all of these measures can be applied.

4.4 | Electric field modelling

FEM packages such as COMSOL have proven to be an indispensable tool in evaluating different designs since they allow prediction of the transformer parameters [7, 11]. The transformer is modelled in 3D FEM to evaluate the electric field distribution and parasitic capacitance. A linear voltage distribution is applied to the secondary winding as shown in Figure 7a.

According to the IEC 60664 standard, clearances on the order of 10 mm can withstand inhomogeneous electric fields up to 0.6–0.7 kV/mm (Table A.1 in [22]). Taking into account approx. 15% derating for the high-frequency voltage, the average electric field should be limited to approx. 0.5 kV/mm to prevent discharges and flashover in air. The field distribution shown in Figure 7b is on the border of meeting this criterion, and HV tests are required to evaluate the PD inception and withstand voltages (see Section 5.4).

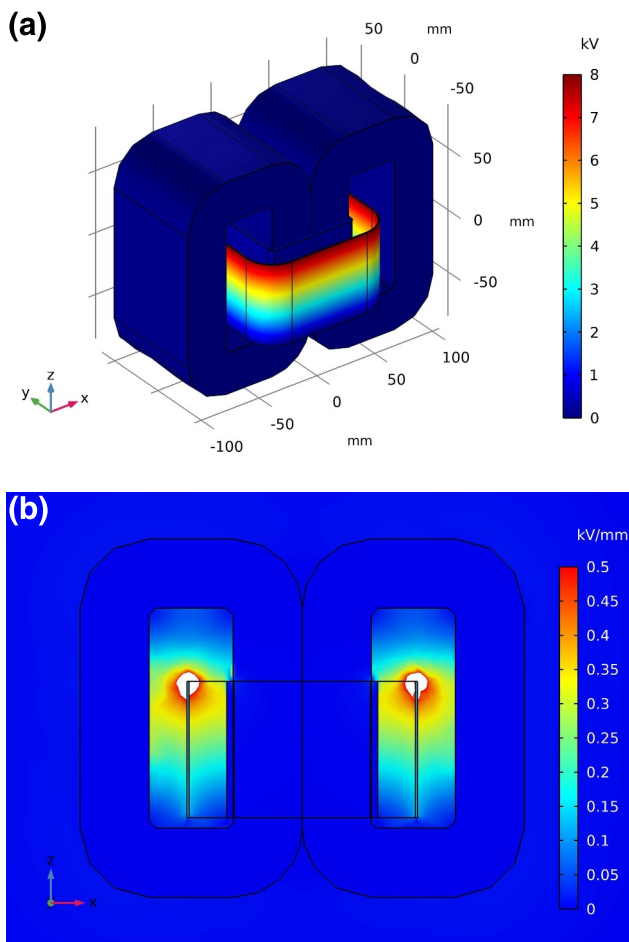


FIGURE 7 Potential distribution (a) and electric field (b) from 3D FEM model of transformer PT3 with 8 kV_p applied to the HV winding.

4.5 | Design procedure

The HF transformer can be designed and evaluated digitally using the tools described in the previous section. Design parameters can be varied easily to reach a transformer with the desired response. A physical prototype is realised and tested afterwards to validate the performance of the transformer.

An HF transformer based on amorphous cut cores is designed and compared to two ferrite-based designs [9, 11] with the goal of reducing the rise time as much as possible while keeping at least 8 kV_p output voltage. The three transformer designs are summarised in Table 3. It is important to note that the parameters for comparison are the output voltage and rise time of the pulse response, irrespective of the size, weight, and cost of the transformer.

The dimensions of PT1 and PT2 can be found in refs. [10, 11]. The geometry and dimensions of PT3 are presented in Figure 8 and Table 4.

5 | EXPERIMENTAL RESULTS

This section presents the experimental results obtained from the three transformers in Table 3. The models are validated through measurements of the frequency response and output pulses, and the differences between the core types are highlighted. The high-voltage performance is evaluated by measuring the PD inception and flashover voltages. The three transformers are shown in Figure 9.

TABLE 3 Transformer designs.

Design	Core	Turns	U_p (V)	f_s (kHz)
PT1	4 × UU 93/152/30 (N87)	4: 200	230	10–50
PT2	8 × UU 126/182/20 (N87)	4: 200	200	10–50
PT3	2 × AMCC1000	3: 60	400	25–100

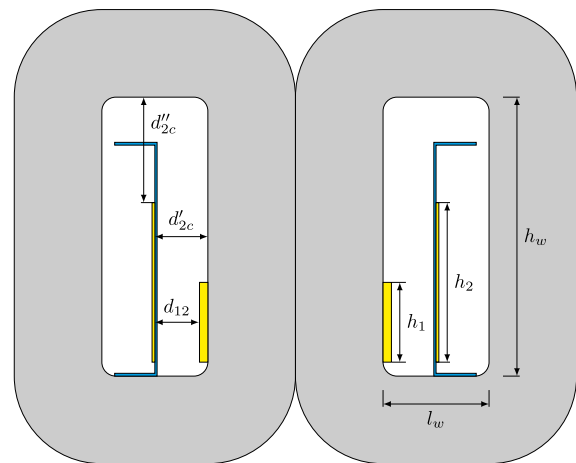


FIGURE 8 Geometry definition of PT3. Core, bobbin, and windings are indicated by grey, blue, and yellow, respectively.

5.1 | Parameter extraction

First, the HF transformer parameters are extracted using the procedure presented in Section 2.3. The parameters matched well with those obtained from the FEM model (capacitances) and through analytical calculation (inductance and resistance). See the comparison in Table 5. The inductances are measured at 10 kHz, whereas the resistances are measured at DC. The secondary leakage inductance L_σ is larger than L_m because it is referred to the secondary side, whereas L_m is referred to the primary.

Note that there is some deviation between the predicted and measured parameters. The magnetising inductance shows a large deviation because of variations in the core material and the small air gap which is always present due to imperfections in the mating surface. The capacitance, on the other hand, can be modelled quite well based on the geometry, resulting in a good match with the measurement.

The main reason L_σ is significantly larger than predicted is the presence of the leads connecting to the primary winding,

which are not considered in the inductance calculation. The increase can be estimated using the inductance of a thin wire in free space, transformed to the secondary side.

$$L_{\sigma,lead} = \ell \mu_0 n^2, \quad (8)$$

where ℓ is the total length of the connecting leads. For PT3, for example, $\ell = 20$ cm and $L_{\sigma,lea} \approx 100$ μ H, resulting in a good agreement between the measurement and analytical calculation. If the leads are twisted or shortened, this inductance may be reduced somewhat.

5.2 | Frequency response

The frequency response of the HF transformers is presented in Figure 10a. This measurement is done without any load (secondary open-circuited) but already provides an indication of the bandwidth. The leakage inductance may be calculated using the parasitic capacitance and resonance frequency.

In Figure 10b, the frequency response of the test setup (HF transformer and damping RC network) is compared against the prediction of the PQR equation. In the considered frequency range, the frequency-dependence of the magnetising inductance and winding resistances are negligible. The deviation at high frequency is due to resonances in the measurement system. The additional loading of the Bode 100 (≈ 55 pF) and the RG58 coaxial cable (≈ 50 pF) reduces the achievable

TABLE 4 Parameters of design PT3.

Part	Parameter	Value
Core	N_c	$2 \times$ AMCC1000
	l_e	422 mm
	A_e	4600 mm ²
	l_w	40 mm
	h_e	105 mm
Primary	N_1	3 turns (foil)
	d_1	0.5 mm
	h_1	65 mm
	d_{12}	17 mm
	N_2	60 turns (solid)
Secondary	d_2	1.0 mm
	h_2	65 mm
	d'_{2c}	21 mm
	d''_{2c}	35 mm

TABLE 5 Extracted transformer parameters.

Parameter	PT1		PT2		PT3	
	Calc.	Meas.	Calc.	Meas.	Calc.	Meas.
L_m (μ H)	315	217	375	280	185	200
L_σ (mH)	6.5	7.3	5.3	5.7	340	440
C_{12} (pF)	2.9	2.9	2.4	3.1	5.1	5.8
C_{22} (pF)	2.1	2.1	1.5	2.0	1.4	1.7
C_σ (pF)	5.0	4.9	3.9	5.1	6.5	7.5
R_{11} (m Ω)	16	15	18	17	5.5	8.4
R_{21} (Ω)	11.8	11.8	42.5	42.6	0.6	0.6



FIGURE 9 Photographs of three transformer designs. (a) Transformer PT1: $A_e = 3360$ mm², $m = 6.0$ kg [9]. (b) Transformer PT2: $A_e = 4480$ mm², $m = 10.4$ kg [11]. (c) Transformer PT3: $A_e = 4600$ mm², $m = 14.2$ kg.

bandwidth. Nevertheless, this comparison demonstrates the validity of the model and the extracted parameters.

5.3 | Pulse response

In Figure 11, the pulse response measured on PT3 is compared to the response predicted by the PQR equation. There is good agreement between measurement and the analytical model. However, the measurement deviates a bit due to unmodelled dynamics of the inverter (DC link oscillation).

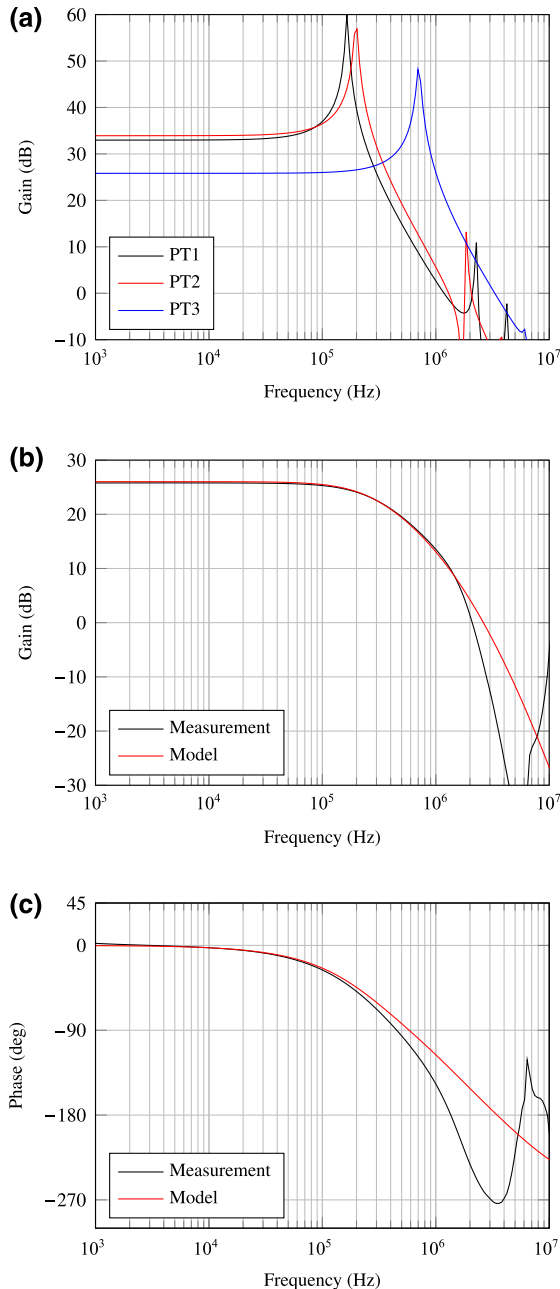


FIGURE 10 Frequency response of HF transformers. (a) Open-circuit response measured with Bode 100. Comparison between model and measured response for PT3 with $C_{DUT} = (68 + 105)$ pF and $R_d = 4$ k Ω , (b) gain and (c) phase.

The rise times of the three transformers are compared in Table 6 with $C_{DUT} = 68$ pF and R_d tuned to give <5% overshoot. The analytical model can predict the rise time with an error of less than 5%.

5.4 | High-voltage withstand test

Because a flashover inside the transformer could destroy the low-voltage PE, the high voltage performance is tested through a 50 Hz AC withstand test. The secondary winding is replaced by copper tape. This is only partially representative since the secondary winding should have a linear voltage distribution, but it indicates the worst case.

The PD inception and flashover voltages are presented in Table 7. They are measured by increasing the voltage in steps of 0.5 kV, maintaining the level for about 30 s to visually check PD on the secondary winding from various angles at a distance of 3–4 m. PD activity is measured optically using a Uvirco CoroCAM 6HD, which has a sensitivity of about 3 pC at 20 m.

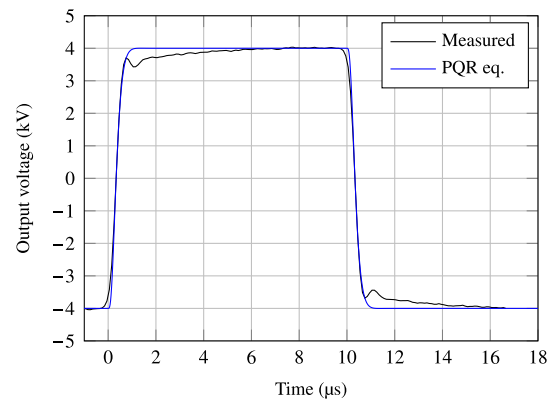


FIGURE 11 Comparison of pulse response simulation and measurements for PT3 with $f_s = 50$ kHz, $C_{DUT} = 68$ pF and $R_d = 4.6$ k Ω .

TABLE 6 Comparison of rise time.

t_r	PT1	PT2	PT3
Analytical model	1.76 μ s	1.59 μ s	465 ns
Measurement	1.70 μ s	1.52 μ s	480 ns
Error	3.5%	4.6%	-3.1%

TABLE 7 High-voltage performance (withstand test).

Design	Test voltage	PDIV U_i	Flashover U_f	Location
PT1	50 Hz sine	10 kV _{rms}	11 kV _{rms}	HV to core
	50 kHz square	7.0 kV _p	—	—
PT2	50 Hz sine	9 kV _{rms}	16 kV _{rms}	HV to core
	50 kHz square	6.5 kV _p	—	—
PT3	50 Hz sine	11 kV _{rms}	14 kV _{rms}	HV to core
	50 kHz square	7.5 kV _p	—	—

5.4.1 | Relation to high-frequency PDIV

The inception voltages in Table 7. For PT3, the PDIV at 50 kHz was measured to be around 7.5 kV_{pk}, meaning that the PDIV is reduced by more than 50% under high-frequency square wave excitation.

This is similar to Agarwal et al., who show that the PDIV is decreased by 30% in the frequency range 10–50 kHz compared to 50 Hz [3]. The leading theory for this phenomenon is based on space charge. After a corona discharge takes place, space charge is deposited in the gas surrounding the electrode. At high frequencies, the space charge cannot fully dissipate before the voltage polarity reversal which results in field enhancement and a lowering of the PDIV compared to 50 Hz sinusoidal voltages [6, 23].

5.4.2 | Window size

In all three cases, the PD activity is localised around the edges of the HV winding (see Figure 12), where the field is concentrated due to the small wire diameter. This effect dominates the PDIV and might be improved by providing an additional layer of insulation, for example, by impregnation of the complete winding with epoxy.

On the other hand, the flashover voltage improves significantly when a core with a larger window is used (see, e.g. the improvement from PT1 to PT2). The highest flashover voltage is obtained when the HV winding is placed in the middle of the window. A trade-off must be made between U_f and the leakage inductance L_σ .

5.4.3 | Amorphous cut cores

Amorphous cut cores (PT3) have no drawbacks regarding high-voltage performance in the voltage range that could be tested. The PDIV and flashover voltage are comparable to

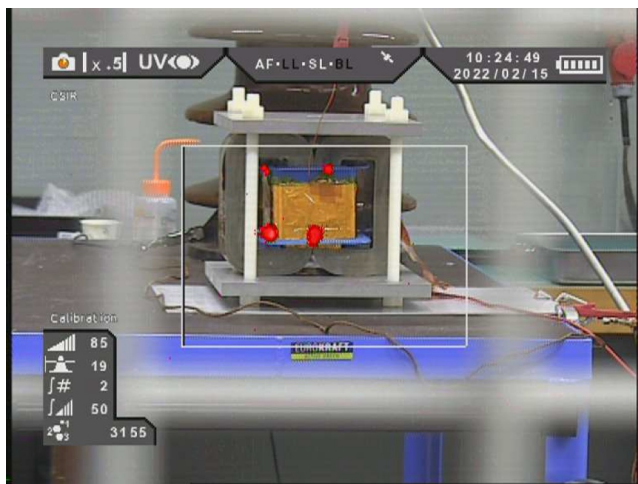


FIGURE 12 CoroCAM photograph showing discharges at the top of the high-voltage winding at 13 kV. Under normal conditions (linear voltage distribution), there would be no discharges at the bottom of the winding.

ferrite and mostly depend on the core and winding geometry. The two main concerns were:

1. Sharp edges are present due to the 25 μm thick ribbons of metal that make up the core. Field enhancement occurs at these locations but is not significant enough to induce PD before flashover.
2. Floating potentials and discharges could arise because the layers of ribbons are insulated from each other. This has not been observed because the core was grounded uniformly.

5.5 | Thermal performance

The ferrite transformers (PT1, PT2) have a core loss of several tens of watts. Given the large size of the transformer, this power can be dissipated effectively to the environment with a negligible temperature rise. On the other hand, the amorphous transformer (PT3) heats up significantly as shown in Figure 13. From the core loss curves presented in Figure 6b, it can be calculated that losses would be 1 kW at the rated output voltage and 25 kHz.

As expected, most of the temperature rise is concentrated around the cut. Two potential explanations are (i) the high conductivity of this area and (ii) the orthogonal flux due to misalignment between the core halves [20].

An improved cooling solution is required to perform insulation tests for an extended time. Short-term tests do not cause a noticeable increase in core temperature because of the large thermal mass of the transformer.

5.6 | Submersion in oil

To ensure that the transformer is discharge-free up to the desired output voltage, it was submerged in Nynas transformer oil. The AC flashover voltage increased to 34 kV_{rms}.



FIGURE 13 Thermal image of HF transformer 3 using an amorphous cut core at $f_s = 50$ kHz, $U_p = 200$ V, and $U_{DUT} = 4$ kV_{pk}. Estimated core losses $P_c = 280$ W. The region around the cut is approx. 30°C hotter than the rest of the core.

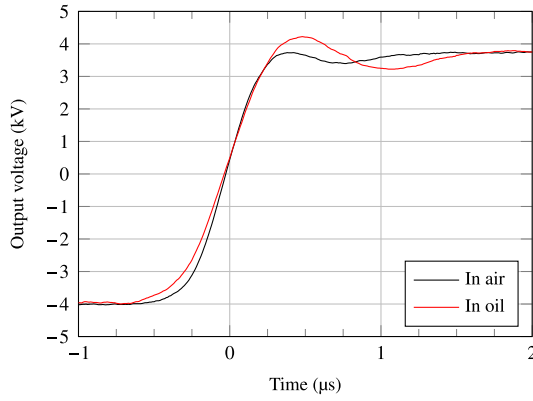


FIGURE 14 Comparison of the measured pulse response with and without transformer oil.

TABLE 8 Rise time and overshoot of PT3 ($C_{DUT} = 68$ pF).

Parameter	In air	In oil	In oil
R_d (k Ω)	4.6	4.6	5.1
Rise time (ns)	480	420	520
Overshoot (%)	0.2	12.7	4.8

Because oil has a dielectric constant of $\epsilon_r \approx 2.4$, the parasitic capacitances will increase by this same factor. Additionally, longer leads are required to supply the primary voltage, increasing the leakage inductance. The impact of these changes on the rise time and overshoot is shown in Figure 14.

As predicted by the analytical model (Figure 4), the increased parasitic capacitance does not degrade the frequency response. The biggest impact is due to the increased parasitic inductance in the primary leads connecting to the inverter. As a result, the desired output voltage of ± 8 kV at 25–100 kHz could be reached with a slight increase in rise time (Table 8). The effect on the overshoot must be carefully considered, since a non-zero overshoot may have a significant impact on the measured lifetime.

Additionally, the oil improves the thermal performance of the transformer by acting as a coolant and adding to the total thermal mass.

5.7 | Limitations

It has been shown that the HF transformer-based setup can achieve suitable square wave voltages with rise times much shorter than the switching period. However, the DUT capacitance is the major limiting factor in the rise time.

With increasing capacitance, the rise time will drop significantly. The damping resistance R_d should be reduced to increase it back to the desired level. This leads to considerable primary current peaks. The peak primary current is calculated using Equation (9), where U_{DUT} is the voltage across the DUT.

TABLE 9 Effect of varying load capacitance (16 kV_{pp}, 50 kHz).

Parameter	Value		
	$C_{DUT} + C_d = 68$ pF, $R_d = 5.1$ k Ω	$C_{DUT} + C_d = 140$ pF, $R_d = 5.1$ k Ω	$C_{DUT} + C_d = 140$ pF, $R_d = 3.1$ k Ω
t_r	520 ns	1.1 μ s	750 ns
I_p	45 A	50 A	62 A
P_{Rd}	990 W	1.9 kW	1.9 kW

$$I_p = n(C_{DUT} + C_d) \frac{dU_{DUT}}{dt} \quad (9)$$

The power P_{Rd} dissipated in R_d is independent of its value and depends only on the peak-to-peak output voltage (including overshoot), the load capacitance, and the repetition frequency. Approximation (10) is valid for $R_d \gg 0$.

$$P_{Rd} \approx f_s (C_{DUT} + C_d) U_{o,pp}^2 \quad (10)$$

Measurement and simulation data are presented in Table 9 for two values of capacitive load and an output voltage of 16 kV_{pp} at 50 kHz.

Therefore, the DUT capacitance is limited by the pulse current capability of the driving inverter and the losses in R_d . For samples with higher capacitance, other high-frequency test methods could be investigated. In some cases, HF sinusoidal voltages (generated by, e.g., a resonant transformer) can be used to evaluate lifetime [2].

6 | DISCUSSION

The main goal of the HF transformer design presented in this paper was to reduce the parasitics of the transformer to achieve square voltage waveforms with short rise times and no overshoot when driving an RC -damped capacitive load.

It has been found that reducing the size of the transformer and inter-winding volume has only a limited effect (compare, e.g., PT1 and PT2) and can impair the high-voltage performance. The most significant improvements can be obtained by reducing the number of turns and the turns ratio, since $L_\sigma \propto N^2$, n^2 . However, to achieve the same peak output voltage, this results in increased volt-seconds applied to the core, necessitating higher B_{sat} .

This paper investigated the application of MetGlas amorphous cut cores with a saturation level of 1.56 T. As expected, the number of turns and turns ratio could be reduced by increasing the primary voltage, resulting in reduced parasitics and a significantly increased bandwidth (1.1 MHz for PT3 vs. 300 kHz for PT2). However, the high losses (core losses and dissipation in R_d) resulted in a thermal limit on the available insulation test voltage, frequency, and duration.

These observations leave two angles of attack for future research on HF transformers based on special magnetic materials:

1. Investigate the reduction of eddy current-induced losses in (amorphous) cut cores. If these losses can be eliminated, thermal performance similar to ferrite cores may be feasible.
2. Nanocrystalline metals have a core loss much lower than amorphous metals while still offering high B_{sat} and μ_r . Considering the high pulse repetition frequency, this could make nanocrystalline cores more suitable for this application.

Regardless of the core material, using more advanced transformer configurations could help achieve lower leakage inductance. For example, the cascade, fractional, and adder configurations discussed by Mangalvedekar et al. [16, 19].

7 | CONCLUSION

In this paper, the application of amorphous cut cores in HV HF transformers has been investigated. High bandwidth and low rise times are achievable because of the low parasitics of the transformer. This improvement over ferrite-based transformers was made possible by the high saturation induction of amorphous metals, enabling a reduction in the number of turns and turns ratio.

The use of amorphous magnetic cores for high-voltage applications has been validated through an AC withstand test. The transformer showed similar PDIV and flashover voltages as the ferrite-based transformers. The high-frequency PDIV can be 50% lower than that measured at 50 Hz, which is resolved by placing the transformer in oil. Short-term tests can be performed with faster rise times than previously demonstrated. However, the amorphous core had excessive core losses, which limited the usable test voltage and duration due to heating of the core.

These results show that, while using high- B_{sat} magnetic cores is advantageous for the frequency response, several challenges must be resolved before they can reach the same level as comparable ferrite-based transformers.

ACKNOWLEDGEMENTS

The authors express their appreciation for the material and financial support of the High Voltage Technology group of the Delft University of Technology and Prodrive Technologies. This project is partly funded by the Dutch TKI Urban Energy programme (grant no. 1821403), which is gratefully acknowledged.

CONFLICT OF INTEREST STATEMENT

The authors declare no potential conflict of interest.

DATA AVAILABILITY STATEMENT

The data that support the findings of this study are available from the corresponding author upon reasonable request.

ORCID

Gijs Lagerweij  <https://orcid.org/0000-0002-1602-757X>
Mohamad Ghaffarian Niasar  <https://orcid.org/0000-0003-1766-8077>

REFERENCES

1. Cavallini, A., Fabiani, D., Montanari, G.C.: Power electronics and electrical insulation systems – Part 1: phenomenology overview. *IEEE Electr. Insul. Mag.* 26(3), 7–15 (2010)
2. Cavallini, A., Fabiani, D., Montanari, G.C.: Power electronics and electrical insulation systems – Part 2: life modeling for insulation design. *IEEE Electr. Insul. Mag.* 26(4), 33–39 (2010)
3. Agarwal, R., et al.: The effects of PWM with high dv/dt on partial discharge and lifetime of medium-frequency transformer for medium-voltage (MV) solid state transformer applications. *IEEE Trans. Ind. Electron.* 70(4), 3857–3866 (2022)
4. Mirza, A., et al.: Modeling electrical aging of polyimide Kapton HN under high-voltage high-frequency pulse waveforms. *IEEE Trans. Dielectr. Electr. Insul.* 29(6), 2394–2401 (2022)
5. Ghassemi, M.: Accelerated insulation aging due to fast, repetitive voltages: a review identifying challenges and future research needs. *IEEE Trans. Dielectr. Electr. Insul.* 26(5), 1558–1568 (2019)
6. Zang, Y., et al.: Optical detection method for partial discharge of printed circuit boards in electrified aircraft under various pressures and voltages. *IEEE Trans. Transport Electric.* 8(4), 4668–4677 (2022)
7. Lagerweij, G.W.: Reliability and Ageing of IMS PCBs in High-Voltage Power Electronic Applications. Delft University of Technology (2023). <http://resolver.tudelft.nl/uuid:c0fd0e4f-10fc-4558-bfd6-1d691a1acc1c>
8. Kulkarni, M.: Design and Prototyping of High Voltage Switch for Arbitrary Waveform Generator. Delft University of Technology (2023). <http://resolver.tudelft.nl/uuid:e292a676-b865-4591-9755-250a92b4bec0>
9. Mathew, P.: Pulsed Ageing of Oil-Paper: Test Modulators and Ageing Trends. Delft University of Technology (2021). <http://resolver.tudelft.nl/uuid:6551068d-3de4-4fb1-9227-31259052e88a>
10. Mathew, P., Niasar, M.G., Vaessen, P.: Design of high-frequency fast-rise pulse modulators for lifetime testing of dielectrics. *IEEE Trans. Dielectr. Electr. Insul.* 30(6), 2798–2808 (2023)
11. Kaparapu, R.K.: Design and Implementation of a Pulse Transformer and Study on Ageing of Oil Impregnated Paper under Pulsed Stresses. Delft University of Technology (2022). <http://resolver.tudelft.nl/uuid:9f1ee452-0e88-4bc7-8179-a246fe705af4>
12. Mathew, P., Niasar, M.G.: Lifetime of oil-impregnated paper under pulse stress at different frequencies. *Proc. Nordic Insul. Symp.* 27(1) (2022)
13. IEEE Standard for Pulse Transformers. ANSI/IEEE Std 390-1987, pp. 1–32 (1987)
14. Candolfi, S., et al.: Efficient parametric identification method for high voltage pulse transformers. In: 19th IEEE Pulsed Power Conf, pp. 1–6 (2013). ISSN: 2158-4923
15. Biela, J., Kolar, J.W.: Using transformer parasitics for resonant converters – a review of the calculation of the stray capacitance of transformers. In: 40th Ind. Appl. Conf., vol. 3, pp. 1868–1875 (2005)
16. Mangalvedekar, H.A., et al.: Ferrite core based pulse power modulator. *IEEE Trans. Dielectr. Electr. Insul.* 18(4), 1158–1162 (2011)
17. Kiran, M.R., et al.: Characterization of the optimized high frequency transformer using nanocrystalline and amorphous magnetic materials. In: 22nd Int. Conf. Electr. Mach. Sys., pp. 1–4 (2019). ISSN: 2642-5513
18. Zhang, S., Chen, D., Bai, B.: Study of a high-power medium frequency transformer using amorphous magnetic material. *Symmetry* 14(10), 2129 (2022)
19. Mangalvedekar, H.A., et al.: Development of solid state pulse power modulator using toroidal amorphous core. *IEEE Trans. Dielectr. Electr. Insul.* 16(4), 1006–1010 (2009)
20. Cougo, B., et al.: Increase of tape wound core losses due to interlamination short circuits and orthogonal flux components. In: 37th Ann. Conf. IEEE Ind. Electr. Soc., pp. 1372–1377. IEEE (2011)
21. Lambert, M., et al.: Analytical calculation of leakage inductance for low-frequency transformer modeling. *IEEE Trans. Power Deliv.* 28(1), 507–515 (2013)
22. IEC TC 109: Insulation Coordination for Equipment within Low-Voltage Systems – Part 1: Principles, Requirements and Tests. International Electrotechnical Commission, 2020. 60664-1 (2020)

23. Zang, Y., et al.: Partial discharge behavior of typical defects in power equipment under multilevel staircase voltage. *IEEE Trans. Dielectr. Electr. Insul.* 29(4), 1563–1573 (2022)
24. Biela, J., Bortis, D., Kolar, J.W.: Modeling of pulse transformers with parallel- and non-parallel-plate windings for power modulators. *IEEE Trans. Dielectr. Electr. Insul.* 14(4), 1016–1024 (2007)

How to cite this article: Lagerweij, G., Niasar, M.G.: Design of a high-frequency transformer based on amorphous cut cores for insulation breakdown testing. *High Voltage.* 1–12 (2024). <https://doi.org/10.1049/hve2.12460>

APPENDIX A

A.1 | Transformer rise time

In Figure 4, it was noted that the rise time shows a dependence on C_σ when L_σ is kept fixed. An example for PT3 is shown in Figure A1. At a specific value C_σ^* , the rise time attains a minimum, after which it increases again. This may be understood by considering the delicate interaction between the transformer ($L_\sigma C_\sigma$) and load ($R_d C_{eq}$).

If $C_\sigma = 0$, the equivalent circuit is a damped series *RLC* circuit, and the rise time is determined by its natural frequency. When introducing C_σ , two critical parameters to consider are (i) the characteristic impedance of the transformer circuit and (ii) the natural frequency of the transformer compared to that of the load. Energy is transferred from C_σ to the output capacitor.

When C_σ is small compared to C_{eq} , the natural frequency of the transformer is much larger than that of the damping filter. A small amount of energy is transferred to C_{eq} every oscillation period. When C_σ increases, the amount of energy that can be transferred becomes larger, leading to a shorter rise time. If C_σ increases further than this sweet spot, the natural

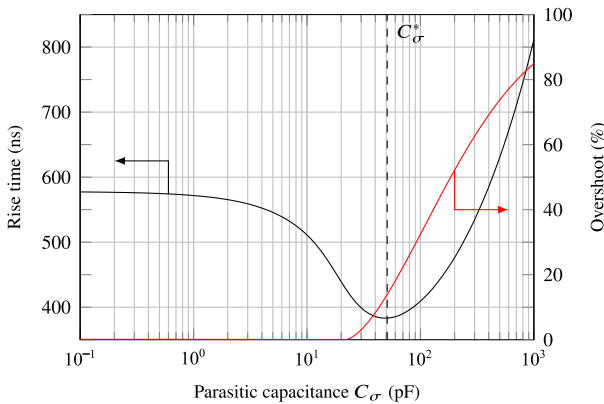


FIGURE A1 Rise time and overshoot versus C_σ for $L_\sigma = 440 \mu\text{H}$, $C_{eq} = 90 \text{ pF}$ and $R_d = 4 \text{ k}\Omega$.

frequency of the transformer becomes similar to or smaller than that of the filter, resulting in an increasing rise time. The transformer parasitics then dominate the rise time. Under conditions different from those described in this paper, such as excess damping or operation with very large or small capacitive loads, the described relations may change. No analytical equation has yet been found relating the rise time to C_σ in a form that is amenable to analysis.

A.2 | PQR equivalent circuit

The equivalent circuit shown in Figure 2 can be transformed into the one shown in Figure 3 by referring the components to the secondary side. Additionally, R_{11} and R_{21} are typically small and do not contribute significantly to the frequency response.

The leakage inductance L_σ is the sum of the primary and secondary leakage inductances as shown in Equation (A1). Quantities with a double prime are referred to the secondary side.

$$L_\sigma = L''_{11} + L_{21} = n^2 L_{11} + L_{21} \quad (\text{A1})$$

Furthermore, the parasitic capacitances can be referred to the secondary side using the conservation of electrostatic energy [14], which yields

$$C''_{11} = \frac{1}{n^2} C_{11} + \frac{1-n}{n^2} C_{12} \quad (\text{A2a})$$

$$C''_{22} = C_{22} + \frac{n-1}{n} C_{12} \quad (\text{A2b})$$

$$C''_{12} = \frac{1}{n} C_{12} \quad (\text{A2c})$$

Next, $C_\sigma = C''_{22} + C''_{12} = C_{22} + C_{12}$ because experiments have shown that C_{11} has a negligible influence on the frequency response. This result is similar to that of Biela et al. [24]. This choice of C_σ gives good results for rise time and overshoot.

A.3 | Parameter extraction

Similarly, the primary-referred capacitances derived from the parameter extraction procedure can be transformed to the equivalent circuit of Figure 2. Quantities with a single prime are referred to the primary.

$$C_{11} = C'_{11} + (n-1)C_{12} \quad (\text{A3a})$$

$$C_{22} = \frac{1}{n^2} C'_{22} + \left(\frac{1}{n} - 1\right) C_{12} \quad (\text{A3b})$$

$$C_{12} = \frac{1}{n} C'_{12} \quad (\text{A3c})$$